



Published in final edited form as:

Anal Chem. 2019 February 19; 91(4): 2994–3001. doi:10.1021/acs.analchem.8b05283.

Characterization and Quantification of Highly Sulfated Glycosaminoglycan Isomers by Gated-TIMS NETD MS/MS

Juan Wei¹, Jiandong Wu¹, Yang Tang^{1,2}, Mark E. Ridgeway³, Melvin A. Park³, Catherine E. Costello^{1,2}, Joseph Zaia¹, and Cheng Lin^{*,1}

¹Center for Biomedical Mass Spectrometry, Boston University School of Medicine, Boston, MA 02118

²Department of Chemistry, Boston University, Boston, MA 02215

³Bruker Daltonics, Billerica, MA 01821, USA

Abstract

Glycosaminoglycans (GAGs) play vital roles in many biological processes, and are naturally present as complex mixtures of polysaccharides with tremendous structural heterogeneity, including many structural isomers. Mass spectrometric analysis of GAG isomers, in particular highly sulfated heparin (Hep) and heparan sulfate (HS), is challenging because of their structural similarity and facile sulfo losses during analysis. Herein, we show that highly sulfated Hep/HS isomers may be resolved by gated-trapped ion mobility spectrometry (gated-TIMS) with negligible sulfo losses. Subsequent negative electron transfer dissociation (NETD) tandem mass spectrometry (MS/MS) analysis of TIMS-separated Hep/HS isomers generated extensive glycosidic and cross-ring fragments for confident isomer differentiation and structure elucidation. The high mobility resolution and preservation of labile sulfo modifications afforded by gated-TIMS MS analysis also allowed relative quantification of highly sulfated heparin isomers. These results show that the gated-TIMS-NETD MS/MS approach is useful for both qualitative and quantitative analysis of highly sulfated Hep/HS compounds in a manner not possible with other techniques.

Graphical abstract

*Corresponding Author: chenglin@bu.edu.

Author Contributions

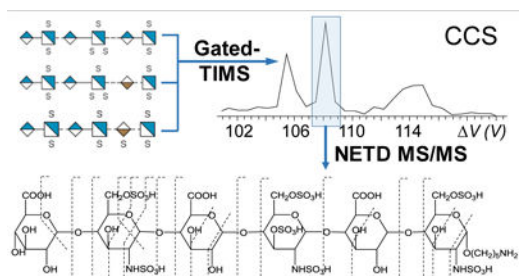
C.L. defined the original concept. J. Wei and Y.T. performed the gated-TIMS MS/MS analysis. J. Wei and J. Wu performed spectral interpretation. M.E.R. and M.A.P. assisted with gated-TIMS implementation on FTICR MS. J. Wei and C.L. coordinated and wrote the manuscript with contributions from all authors. All authors have given approval to the final version of the manuscript.

ASSOCIATED CONTENT

Supporting Information

The Supporting Information is available free of charge on the ACS Publications website. Figure S-1, structures of the synthetic GAG standards used in this study; Figure S-2, EIMs of Compound 3 ($[M-3H]^{3-}$) and its sulfo loss products under different experimental conditions; Figure S-3, MS of Compound 3 with different ESI solvent compositions; Figures S-4 and S-5, EIMs of each isomer in several charge states; Figure S-6 and S-7, NETD fragmentation maps of each isomer ($[M-3H]^{3-}$) following gated-TIMS separation; Figure S-8, zoomed-in regions of the NETD spectra of Compounds 3 and 4 ($[M-3H]^{3-}$); Table S-1, typical instrument parameters used for gated-TIMS MS analysis; Tables S-2 to S-6, lists of assigned peaks in the NETD spectra of each gated-TIMS-separated isomer; Table S-7, Data used to generate the quantitative analysis plot shown in Figure 5 (PDF)

The authors declare no competing financial interest.



Glycosaminoglycans (GAGs) are linear polysaccharides consisting of disaccharide repeats with alternating amino sugar and hexuronic acid (HexA) or galactose units. Through interaction with their protein binding partners, GAGs are involved in many biological processes including cell signaling, inflammation, cell proliferation, and tumor metastasis.^{1–12} Heparin (Hep) and heparan sulfate (HS) are GAGs with a high degree of sulfation, and among the most acidic biomolecules found in nature. The electrostatic interaction between Hep/HS and protein ligands is modulated by their sulfation pattern, and plays a key role in their biological functions. For example, binding between antithrombin and a pentasaccharide sequence containing a critical 3-*O* sulfation on the central glucosamine (GlcN) residue is essential for the anti-coagulation activity of Hep/HS.^{13,14} Heparins also mediate recognition between fibroblast growth factors (FGFs) and their receptors, thereby regulating cell proliferation.^{15–18} Whereas FGF-2 preferentially interacts with tetra- and hexasaccharide sequences containing the -IdoA2S-GlcNS- motif (IdoA = iduronic acid), FGF-1 has a strong affinity to the -IdoA2S-GlcNS6S- motif. Heparins containing 6-*O* sulfation display anti-inflammatory properties by interfering with P- and L-selectin-initiated cell adhesion.⁵ Despite the strong correlation between the GAG structures and their biological functions, subtle structural differences are often difficult to track, and full characterization of GAGs, especially the highly sulfated Hep/HS glycans, remains a significant analytical challenge.

Although all Hep/HS saccharides share the same HexA(1→4)-GlcN(α 1→4)- disaccharide sequence repeats, the number of Hep/HS structures is multiplied by the variation in the number of repeating units, the hexuronic acid stereochemistry, and the pattern of *N*-acetylation and sulfation, resulting in tremendous structural diversity and the common occurrence of isomers.¹⁹ GAG analysis often requires enzymatic digestion or chemical depolymerization to break down polysaccharide chains into shorter oligosaccharides with degrees of polymerization (dp) ranging from dp2 to dp20. The Hep/HS digests are then analyzed by mass spectrometry (MS), usually in conjunction with liquid chromatography (LC). The extent and pattern of sulfation in the original Hep/HS chains can be estimated by relative quantitation of all oligosaccharides.

Isomeric Hep/HS structures may be separated by capillary electrophoresis (CE),^{20–22} or by LC, including reversed phase-ion pairing (RP-IP) chromatography, hydrophilic interaction liquid chromatography (HILIC), strong anion exchange (SAX) chromatography, and porous graphitized carbon (PGC) chromatography.^{23–27} Among these, SAX offers the highest isomer resolving power, but is incompatible with direct MS analysis due to the high concentration of nonvolatile salt used in the elution buffer. An alternative, volatile salt cetyltrimethylammonium (VSCTA)-SAX, uses the buffer ammonium bicarbonate that can

be easily removed by evaporation, thus allowing effective subsequent analysis by offline electrospray MS. Meanwhile, superior isomer resolution of HS oligosaccharides was recently demonstrated by Miller *et al.* with online PGC-LC-MS/MS analysis.²⁷ However, there are concerns over PGC column stability and reproducibility, and the formation of ammonium adducts leading to increased precursor heterogeneity.

Ion mobility spectrometry²⁸ has emerged as a powerful alternative for separation of isomeric structures, including GAG isomers.^{29–35} IMS complements LC in that it is a post-ionization, gas-phase separation method, wherein analyte ions are sorted based on their size, charge and shape. Isomers may differ in collisional cross section (CCS), and therefore ion mobilities, depending on their gas-phase conformations. IMS analysis is generally faster than LC and can be easily coupled to MS. Moreover, the CCS of an analyte ion is an additional property which can be used for its identification.

Significant progress in GAG structural characterization has been made through the development of electron activated dissociation (ExD) tandem MS (MS/MS) methods.^{36–42} In particular, electron detachment dissociation (EDD)^{37,38} and negative electron transfer dissociation (NETD)^{39–42} are capable of generating extensive glycosidic and cross-ring cleavages while preserving labile sulfate modifications in highly sulfated GAGs, thus allowing sequence determination and sulfation site localization. Differentiation of C5 epimers, IdoA and GlcA (glucuronic acid), by EDD and NETD has also been demonstrated.^{36,43} EDD MS/MS has been used in conjunction with high-field asymmetric-waveform ion mobility spectrometry (FAIMS) to separate and characterize epimeric HS tetrasaccharides.³² However, FAIMS does not provide CCS measurement, as it separates ions based on their differential mobilities in strong and weak electric fields. The applications of FAIMS are restricted by its relatively low sensitivity and limited peak capacity that result from diffusion and harsh discrimination against high-mobility ions.⁴⁴

EDD and NETD MS/MS analyses are performed on a timescale longer than the conventional drift-time IMS separation. It is possible to couple IMS separation with slower analysis methods when the IMS device is used as a mobility filter.^{45,46} Trapped ion mobility spectrometry (TIMS)^{47,48} offers high mobility resolution and ion transmission efficiency, and has shown great promise in isomer separations.^{49–52} Successful coupling of TIMS to Fourier-transform ion cyclotron resonance (FTICR) MS has been achieved under the selected accumulation (SA)-TIMS mode, and applied to characterization of isomeric glycan mixtures.⁵³ However, SA-TIMS requires extended ion storage time in the TIMS analyzer, leading to significant ion heating and is therefore not suitable for analysis of labile compounds or compounds whose conformers may interconvert during the storage time. Such limitation may be overcome by gated-TIMS where ions of a given mobility are selected by an electrical gate and accumulated in a low-pressure collision cell.^{54,55} Here, we present our initial results on the gated-TIMS coupling to NETD MS/MS and demonstrate its utility for characterization and quantification of isomeric Hep/HS oligosaccharides.

EXPERIMENTAL SECTION

Materials

GAG standards, GlcA-GlcNAc6S-IdoA-GlcNAc6S-(CH₂)₅-NH₂ (Compound 1), GlcA-GlcNAc-IdoA2S-GlcNAc6S-(CH₂)₅-NH₂ (Compound 2), GlcA-GlcNS6S-GlcA-GlcNS3S6S-GlcA-GlcNS6S-(CH₂)₅-NH₂ (Compound 3), GlcA-GlcNS6S-GlcA-GlcNS3S6S-IdoA-GlcNS6S-(CH₂)₅-NH₂ (Compound 4), and GlcA-GlcNS6S-GlcA-GlcNS6S-IdoA2S-GlcNS6S-(CH₂)₅-NH₂ (Compound 5) were synthesized by the Boons group at the University of Georgia as described previously;⁵⁶ their structures and symbol nomenclature for glycans (SNFG) representations are shown in Supplementary Figure S1. All GAG standards were alkylated at the reducing end via an α -linkage, to facilitate fragment assignment and eliminate anomerism-induced conformational heterogeneity. All other chemicals were purchased from Sigma-Aldrich (St. Louis, MO, USA).

Gated-TIMS-MS and Gated-TIMS-NETD MS/MS Analyses

All experiments were carried out on a Bruker 12-T solariX FTICR mass spectrometer equipped with a prototype TIMS device (Bruker Daltonics, Billerica, MA). GAGs were dissolved in 75:25 water:acetonitrile with 0.1% formic acid to a concentration of around 5 pmol/ μ L except for the quantitative analysis, where Compounds 3 and 4 were mixed at ratios of 20:1, 10:1, 2:1, 1:1, 1:2, 1:10, and 1:20, respectively, with concentrations ranging from 5 to 100 pmol/ μ L. Around 5 μ L of sample was loaded into a pulled glass capillary tip with a 1- μ m orifice diameter, and introduced into the mass spectrometer via static nano-electrospray. The schematic of the TIMS device and the principle of the gated-TIMS operation were described in detail previously.⁵⁴ Briefly, ions entering the TIMS funnel were trapped radially by an RF potential (190 V_{pp}), and axially by an electric field gradient (EFG) at positions where their drift velocity equals the carrier gas flow velocity. Following a 9-ms trapping event, the strength of the axial electric field was gradually decreased by ramping the TIMS analyzer entrance potential from 250 V to -50 V to allow elution of ions in the order of ascending mobilities. A downstream ion gate was pulsed open to allow only ions of selected mobility to pass through and be accumulated in the collision cell. For MS/MS analysis, ions of a given mobility were mass selected by a quadrupole before entering the collision cell. The drift gas (nitrogen) pressure was regulated between 2.5 and 2.7 mbar, depending on the mobility resolution needed. A mixture of perfluoroalkyl phosphazine standards (Agilent Technologies, Santa Clara, CA, USA) was used to generate the mobility calibration curve for CCS calculation. For NETD experiments, fluoranthene cation radicals were generated by a chemical ionization source with argon as the buffer gas. A reagent accumulation time of 200 to 500 ms and a reaction time of 50 to 100 ms were typically used.

Data Analysis

All spectra were processed by DataAnalysis 4.4 (Bruker, Bremen, Germany), and interpreted manually assisted by GlycoWorkbench.⁵⁷ Fragments were annotated according to the Domon and Costello nomenclature.⁵⁸

RESULTS AND DISCUSSION

Reduced ion heating during gated-TIMS analysis

TIMS is commercially available only on time-of-flight MS instruments, as separation occurs on the millisecond timescale thus is more easily coupled to a fast mass analyzer. TIMS coupling to slower analysis methods, such as ExD-FTICR MS/MS, was first accomplished by modifying the axial EFG profile to include an electric field plateau for selective accumulation of ions with the desired mobility inside the TIMS tunnel, as implemented in SA-TIMS.⁵³ However, prolonged ion accumulation during SA-TIMS (hundreds of milliseconds) can result in the radial ion cloud expansion and multipole storage assisted dissociation (MSAD) that has been investigated by the groups of Håkansson and Hofstadler.^{59–61} In contrast, gated-TIMS involves a short ion accumulation time in the TIMS tunnel (around 10 ms), and multiple collision cell fills are used to increase the abundance of ions of the desired mobility and to match the timescale of FTICR MS analysis. The collision cell has a much higher space charge capacity and lower gas pressure ($\sim 10^{-3}$ mbar), and, consequently, ion storage here minimizes MSAD. Suppression of lower-abundance ions of interest in the collision cell is not an issue following mobility selection and m/z filtering.

The advantage of gated-TIMS over SA-TIMS for analysis of labile compounds is illustrated in Figure 1 and Supplementary Figure S2, showing the influence of the TIMS accumulation time on the extent of sulfo losses from a highly sulfated HS hexasaccharide (Compound 3). Although extensive sulfo losses were observed when the TIMS accumulation time exceeded 100 ms (Figure 1d, e), sulfo loss was negligible with a 10-ms TIMS accumulation time even after 600 cycles of collision cell fills (Figure 1f). It appears that the sulfo losses that did occur took place primarily inside the TIMS tunnel, as the majority of sulfo-loss fragment ions did not co-elute with the precursor (Figure S2c, d, bottom panels). Multiple peaks observed in the extracted ion mobiligrams (EIMs) of fragments may have resulted from loss of sulfo group(s) from different sulfation sites, and/or the presence of multiple conformers. Another advantage of gated-TIMS is that the reduced ion storage time minimizes conformational changes. Conformational heating at longer fill/trap times was previously reported for TIMS-TOF MS analysis of ubiquitin ions.⁶² Whereas a single peak existed in the EIMs of the $[M-3H]^{3-}$ species (eluting at 108 V) when the TIMS accumulation time was 10 ms, a second peak with a higher CCS was observed at 110 V when the accumulation time exceeded 50 ms, likely due to heating and unfolding (Supplementary Figure S2, top panel). Thus, gated-TIMS is well-suited for analysis of highly sulfated GAGs, as it preserves labile modifications and minimizes conformational heterogeneity.

Separation of GAG isomers by gated-TIMS

Apart from facile sulfo losses, challenges in MS analysis of GAGs may also arise due to the presence of precursor ions in a range of charge states and cation-adducted forms. Distribution of analytes into multiple species dilutes the signal and complicates the MS analysis. Ammonium adduction is very common in LC-MS analysis of GAGs because of the use of ammonium salt in the elution buffer. In contrast, for IM-MS analysis with direct infusion, the ionization conditions, including the pH and composition of the ESI solution, can be easily manipulated to control the charge state distribution and cation adduction.

Supplementary Figure S3 shows that the addition of 0.1% formic acid significantly reduced cation adduction. The analyte charge states also affect the performance of mobility separation and the NETD spectral quality. Though the NETD efficiency increases with the precursor ion charge state, GAG isomers in higher charge states tend to produce more extended and thus similar gas-phase structures that are difficult to resolve by IMS. Rapid survey scans at relatively low mobility resolution may be first performed to identify the best conditions for separation of isomeric structures. The instrument parameters can then be tuned for higher-resolution scans within targeted mobility ranges. Typical gated-TIMS operating parameters are summarized in Supplementary Table S1.

Survey scans of Compounds 1 and 2 (Supplementary Figure S4) suggested that these two tetrasaccharide (dp4) isomers with a moderate degree of sulfation may be resolved in both 2- and 3- charge states. A high-resolution scan was then performed for the 3- charge state because of its potential to generate more informative NETD spectra. Baseline resolution was achieved for this pair of isomers that differ by the location of one sulfo group (Figure 2a). Likewise, three hexasaccharide (dp6) isomers with a high degree of sulfation, differing in either the location of one sulfo group (Compounds 4 and 5) or the epimeric configuration of a single uronic acid residue (Compounds 3 and 4), were fully resolved in the 3- charge state (Figure 2b). In contrast, higher charge states (4- and 5-) of these dp6 isomers have similar mobilities and cannot be fully resolved (Supplementary Figure S5).

The x-axis of the EIMs shown displays the elution voltage, or the potential drop across the TIMS analyzer ($V = V_{tunnel} - V_{exit\ funnel}$), at the time of elution. The CCS value of each compound (Figure 2, bottom panel) could be calculated based on its elution voltage using a calibration curve established with a series of compounds of known mobilities.⁴⁷ The CCS of an analyte is a fixed value when measured under the same conditions, and can be stored in a database for future reference. Here, the high mobility resolving power offered by gated-TIMS was essential for resolution of isomers with CCS values differing by as little as 2%. Note that the elution voltages of some isomers, when analyzed in the mixture, were slightly different from their respective elution voltages, when analyzed individually. These small shifts likely resulted from the run-to-run pressure fluctuation inside the TIMS tunnel, but were generally less than 0.5%.

Gated-TIMS NETD MS/MS analysis of dp4 isomers

Unlike SA-TIMS, ions of the desired mobility occupy only a small section of the mobility analyzer during the gated-TIMS operation.

External accumulation of ions of interest via multiple collision cell fills may be performed to increase the ion abundance for effective ExD analysis. The impact of multiple fill cycles on the analysis speed can be minimized with accumulation during detection (ADD), where ion accumulation is performed in parallel with MS analysis of the previous ion packet in the ICR cell. In the analyses whose results are shown here, 600 to 900 fill cycles were used prior to NETD. For structural characterization, each mobility- and mass-selected isomer was subjected to NETD in the collision cell.

Figure 3 shows the NETD tandem mass spectra of the two TIMS-isolated dp4 isomers, and their fragmentation patterns are shown in Supplementary Figure S6. Peak assignment was facilitated by the high-mass accuracy FTICR MS measurement and the presence of the reducing-end amionpentyl group. Lists of all assigned fragments can be found in Supplementary Tables S2 and S3. NETD generated many glycosidic and cross-ring fragments without sulfo losses, including several fragment ions unique to each isomer (highlighted in color). In both spectra, the presence of Y_1 and Z_1 ions containing one sulfo group may be used to assign one sulfation site to the reducing-end GlcNAc residue. The second sulfation site may be localized to the internal GlcNAc residue for isomer 1, based on the mass difference between its Y_3^{2-} (or Z_3^{2-}) fragment ion (with 2S) and Y_2 (or Z_2) fragment ion (with 1S) (Figure 3a), and to the internal IdoA residue for isomer 2, based on the mass difference between its C_2 (with no S) and C_3-2H (with 1S) ions (Figure 3b). The sulfation site at the terminal GlcNAc residue can be defined at the 6-*O* position in each isomer, based on the observation of a $^{3,5}A_4$ ion with two sulfo groups; likewise, the second sulfo group in isomer 1 can be assigned to the 6-*O* position of the internal GlcNAc residue, based on the presence of a $^{3,5}A_2$ ion with one sulfo group. Definitive evidence for the exact location of the sulfo group on the IdoA residue of isomer 2 is not present in the spectrum shown here, but this sulfo group is presumed to be located at the 2-*O* position based on known biosynthetic pathways. Thus, peaks 1 and 2 in the EIM of the dp4 mixture can be assigned to Compounds 1 and 2, respectively.

Gated-TIMS NETD MS/MS analysis of highly sulfated dp6 isomers

Characterization of the dp6 mixture presents a bigger challenge. First, it is difficult to achieve complete deprotonation on these highly sulfated compounds, with the result that proton-mediated facile sulfo losses can occur easily during ionization, mobility analysis, and ion transfer. Second, the presence of many sulfate and carboxyl groups resulted in a broad charge state distribution and the formation of many sodiated and ammonium-adducted forms. This complicates subsequent MS/MS analyses. Third, although it is preferable to characterize precursor ions in higher charges states due to their higher NETD efficiency, these dp6 isomers could not be fully resolved in 4- and 5- charge states (Figure S2). To overcome these challenges, the instrument parameters and the ESI solvent composition had to be optimized to minimize cation adduction (Figure S3) and sulfo losses and then the 3-charge state was chosen for NETD analysis, as all three isomers could be mobility resolved in this charge state.

The NETD spectra of the mobility-selected dp6 isomers are shown in Figure 4a-c, and their fragmentation patterns are shown in Supplementary Figure S7. Lists of all assigned fragments can be found in Supplementary Tables S4-S6. In the NETD spectra of peaks 1 and 2 (Figure 4a, b), the Y_2 ions contain only two sulfate groups. This, along with the presence of Y_3 and Z_3 ions with five sulfate groups, suggests that the second GlcN residue is fully sulfated. In contrast, in the NETD spectrum of peak 3 (Figure 4c), the mass difference between its Y_1 (with 2 S) and Y_2 (with 3 S) ions indicates that the HexA residue near the reducing end is singly sulfated, agreeing with the structure of Compound 5. This assignment is confirmed by the presence of high-abundance Z_2-COOH , and $^{1,5}X_2$ ions with three sulfate groups, and a B_5^{2-} fragment with five sulfate groups. Thus, it is relatively easy to distinguish

the sulfation positional isomer, Compound 5 from Compounds 3/4, based on their NETD spectra.

Distinction between the other two compounds, presumably the stereoisomeric Compounds 3 and 4, is more difficult. For both isomers, it is possible to locate all sulfation sites based on the presence of complete series of glycosidic fragments, and $^{3,5}A$ and $^{0,2}A$ ions at the first and third GlcNAc residues (Figure S7). Although MS is often considered blind to chirality, diastereomers, such as epimeric isomers, may sometimes be differentiated by MS/MS based on unique fragmentation patterns associated with each stereochemical configuration.^{36,38,63–65} Amster and coworkers showed that the C5 uronic acid stereochemistry near the reducing end in HS tetrasaccharides may be determined by EDD MS/MS, based on the differential ratio (DR), $DR = \log(1/3((B_3, Y_1, C_2, Z_2)/(Y_2, ^{1,5}X_2)))$, where a positive DR value is associated with GlcA and a negative value with IdoA.³⁶ Even though this strategy cannot be directly applied to determine the epimeric configuration in the compounds studied here, because of the difference in the chain length, charge state and the fragmentation method employed, the DR value may still be used for differentiation. Here, the $^{1,5}X_2$ ions are not observed, and the Y_2 ions have similar abundances, whereas fragments resulting from glycosidic cleavages at the reducing end side of the epimeric center, namely, Y_1 , Z_1 , B_5^{2-} , and C_5^{2-} ions (labeled in green in Figure 4b) are about 2 to 5 times more abundant in the NETD spectrum of peak 2 than in that of peak 1 (Figure S8). As peaks 2 and 1 correspond to GlcA₅-containing Compound 3 and IdoA₅-containing Compound 4, respectively, based on the elution time observed for individual dp6 standards, it appears that glycosidic cleavages on the reducing end side of GlcA, are more prevalent than those next to IdoA. Moreover, the abundance of the cross-ring fragment, $^{0,2}X_4^{2-}$, is eight times greater in Figure 4b than in Figure 4a, suggesting that the epimeric configuration can influence fragmentation distant from the stereochemical center, potentially providing additional information for epimer differentiation. Thus, it is possible to assign these two stereoisomers either by comparing their CCS values to those of the standards (Figure 2b) or by their NETD fragmentation patterns. Here, gated-TIMS NETD MS/MS analysis provided both CCS values and the fragmentation data to enable confident identification.

Relative quantification of isomers by gated-TIMS FTICR MS

Characterization of a highly heterogeneous GAG mixture via a bottom-up approach requires not only identification of oligosaccharides present in its digest, but also their relative quantification. However, highly sulfated GAG isomers are difficult to resolve chromatographically, and facile sulfo losses further complicate the analysis. We showed earlier that gated-TIMS could resolve highly sulfated Hep/HS isomers with negligible sulfo losses. Here, two stereoisomers, Compounds 3 and 4, were mixed at ratios ranging from 20:1 to 1:20 and subjected to nanoESI-gated-TIMS FTICR MS analysis. With a mobility resolution of around 200, these two compounds were baseline resolved in the 3- charge state. Figure 5 shows that the peak area ratio, $A_3/(A_3+A_4)$, scales linearly with the fraction of Compound 3 in the mixture, $C_3/(C_3+C_4)$, thus demonstrating the feasibility of using gated-TIMS MS for relative quantification of GAG isomers. In conjunction with the NETD MS/MS analysis, it is now possible to achieve both identification and quantification of highly sulfated GAG isomers.

CONCLUSIONS

To meet the challenges of GAG analysis, a high-resolution ion mobility separation technique, gated-TIMS, was integrated with NETD, a dissociation method that preserves labile modifications, and high mass resolution FTICR MS, for characterization of highly sulfated GAG isomers. Compared with SA-TIMS, gated-TIMS showed superior performance in preserving the labile sulfo groups, while retaining the ability to resolve isomeric structures, and was also compatible with FTICR analysis. Synthetic dp4 and dp6 standards, including sulfation positional isomers and IdoA/GlcA stereoisomers, could be baseline resolved by gated-TIMS, and their CCS values could be measured and stored for future reference. Online gated-TIMS NETD MS/MS generated extensive fragmentation with a high degree of sulfo retention for detailed structural characterization, along with many diagnostic fragments for isomer differentiation. Relative quantification of highly sulfated Hep/HS isomers was demonstrated for the first time, aided by the high mobility resolution and the soft analysis conditions of gated-TIMS-NETD MS/MS. Coupling of gated-TIMS with NETD MS/MS appears to be a powerful tool for qualitative and quantitative analysis of highly sulfated GAGs.

Supplementary Material

Refer to Web version on PubMed Central for supplementary material.

ACKNOWLEDGMENT

This research is supported by the NIH grants P41 GM104603, R21 GM122635, R21 CA199845, U01CA221234, and S10 RR025082, and National Natural Science Foundation of China (21728501). The authors thank Prof. Geert-Jan Boons for providing the synthetic GAG standards. The contents are solely the responsibility of the authors and do not represent the official views of the awarding offices.

REFERENCES

- (1). Pomin VH Solution NMR conformation of glycosaminoglycans Prog. Biophys. Mol. Biol. 2014, 114, 61–68. [PubMed: 24560989]
- (2). Dam G. B.t.; Kurup S.; van de Westerlo EMA.; Versteeg EMM.; Lindahl U; Spillmann D.; van Kuppevelt TH 3-O-Sulfated Oligosaccharide Structures Are Recognized by Anti-heparan Sulfate Antibody HS4C3 J. Biol. Chem. 2006, 281, 4654–4662. [PubMed: 16373349]
- (3). Misek DE; Patwa TH; Lubman DM; Simeone DM Early detection and biomarkers in pancreatic cancer J. Natl. Compr. Canc. Netw. 2007, 5, 1034–1041. [PubMed: 18053427]
- (4). Guerrini M; Beccati D; Shriver Z; Naggi AM; Bisio A; Capila I; Lansing J; Guglieri S; Fraser B; Al-Hakim A; Gunay S; Viswanathan K; Zhang Z; Robinson L; Venkataraman G; Buhse L; Nasr M; Woodcock J; Langer R; Linhardt R, et al. Oversulfated Chondroitin Sulfate is a major contaminant in Heparin associated with Adverse Clinical Events Nat. Biotechnol. 2008, 26, 669–675. [PubMed: 18437154]
- (5). Wang L; Brown JR; Varki A; Esko JD Heparin's anti-inflammatory effects require glucosamine 6-O-sulfation and are mediated by blockade of L- and P-selectins J. Clin. Investig. 2002, 110, 127–136. [PubMed: 12093896]
- (6). Kelton JG; Warkentin TE Heparin-induced thrombocytopenia: a historical perspective Blood 2008, 112, 2607–2616. [PubMed: 18809774]
- (7). Yayon A; Klagsbrun M; Esko JD; Leder P; Ornitz DM Cell surface, heparin-like molecules are required for binding of basic fibroblast growth factor to its high affinity receptor Cell 1991, 64, 841–848. [PubMed: 1847668]

- (8). Turner N; Grose R Fibroblast growth factor signalling: from development to cancer *Nat. Rev. Cancer* 2010, 10, 116–129. [PubMed: 20094046]
- (9). Monneau Y; Arenzana-Seisdedos F; Lortat-Jacob H The sweet spot: how GAGs help chemokines guide migrating cells *J. Leukoc. Biol.* 2016, 99, 935–953. [PubMed: 26701132]
- (10). Mulloy B; Hogwood J; Gray E; Lever R; Page CP Pharmacology of Heparin and Related Drugs *Pharmacol. Rev.* 2016, 68, 76–141. [PubMed: 26672027]
- (11). Weiss RJ; Esko JD; Tor Y Targeting heparin and heparan sulfate protein interactions *Org. Biomol. Chem.* 2017, 15, 5656–5668. [PubMed: 28653068]
- (12). Bishop JR; Schuksz M; Esko JD Heparan sulphate proteoglycans fine-tune mammalian physiology *Nature* 2007, 446, 1030–1037. [PubMed: 17460664]
- (13). Petitou M; Casu B; Lindahl U 1976–1983, a critical period in the history of heparin: the discovery of the antithrombin binding site *Biochimie* 2003, 85, 83–89. [PubMed: 12765778]
- (14). Jin L; Abrahams JP; Skinner R; Petitou M; Pike RN; Carrell RW The anticoagulant activation of antithrombin by heparin *Proceedings of the National Academy of Sciences* 1997, 94, 14683–14688.
- (15). Pellegrini L Role of heparan sulfate in fibroblast growth factor signalling: a structural view *Current Opinion in Structural Biology* 2001, 11, 629–634. [PubMed: 11785766]
- (16). Shriver Z; Capila I; Venkataraman G; Sasisekharan R Heparin and heparan sulfate: analyzing structure and microheterogeneity *Handb. Exp. Pharmacol.* 2012, 159–176. [PubMed: 22566225]
- (17). Zhao Y; Singh A; Xu Y; Zong C; Zhang F; Boons G-J; Liu J; Linhardt RJ; Woods RJ; Amster IJ Gas-Phase Analysis of the Complex of Fibroblast Growth Factor 1 with Heparan Sulfate: A Traveling Wave Ion Mobility Spectrometry (TWIMS) and Molecular Modeling Study *J. Am. Soc. Mass. Spectrom.* 2017, 28, 96–109. [PubMed: 27663556]
- (18). Kreuger J; Salmivirta M; Sturiale L; Giménez-Gallego G; Lindahl U Sequence Analysis of Heparan Sulfate Epitopes with Graded Affinities for Fibroblast Growth Factors 1 and 2 *J. Biol. Chem.* 2001, 276, 30744–30752. [PubMed: 11406624]
- (19). Safaiyan F; Lindahl U; Salmivirta M Structural Diversity of N-Sulfated Heparan Sulfate Domains: Distinct Modes of Glucuronyl C5 Epimerization, Iduronic Acid 2-O-Sulfation, and Glucosamine 6-O-Sulfation *Biochemistry* 2000, 39, 10823–10830. [PubMed: 10978168]
- (20). Ruiz-Calero V; Moyano E; Puignou L; Galceran MT Pressure-assisted capillary electrophoresis–electrospray ion trap mass spectrometry for the analysis of heparin depolymerised disaccharides *J. Chromatogr. A* 2001, 914, 277–291. [PubMed: 11358222]
- (21). Zamfir AD Applications of capillary electrophoresis electrospray ionization mass spectrometry in glycosaminoglycan analysis *Electrophoresis* 2016, 37, 973–986. [PubMed: 26701317]
- (22). Sanderson P; Stickney M; Leach FE; Xia Q; Yu Y; Zhang F; Linhardt RJ; Amster IJ Heparin/heparan sulfate analysis by covalently modified reverse polarity capillary zone electrophoresis–mass spectrometry *J. Chromatogr. A* 2018, 1545, 75–83. [PubMed: 29501428]
- (23). Melmer M; Stangler T; Premstaller A; Lindner W Comparison of hydrophilic–interaction, reversed-phase and porous graphitic carbon chromatography for glycan analysis *J. Chromatogr. A* 2011, 1218, 118–123. [PubMed: 21122866]
- (24). Doneanu CE; Chen W; Gebler JC Analysis of Oligosaccharides Derived from Heparin by Ion-Pair Reversed-Phase Chromatography/Mass Spectrometry *Anal. Chem.* 2009, 81, 3485–3499. [PubMed: 19344114]
- (25). Gill VL; Aich U; Rao S; Pohl C; Zaia J Disaccharide Analysis of Glycosaminoglycans Using Hydrophilic Interaction Chromatography and Mass Spectrometry *Anal. Chem.* 2013, 85, 1138–1145. [PubMed: 23234263]
- (26). Miller RL; Guimond SE; Shivkumar M; Blocksidge J; Austin JA; Leary JA; Turnbull JE Heparin isomeric oligosaccharide separation using volatile salt strong anion exchange chromatography *Anal. Chem.* 2016, 88, 11542–11550. [PubMed: 27801575]
- (27). Miller RL; Guimond SE; Prescott M; Turnbull JE; Karlsson N Versatile Separation and Analysis of Heparan Sulfate Oligosaccharides Using Graphitized Carbon Liquid Chromatography and Electrospray Mass Spectrometry *Anal. Chem.* 2017, 89, 8942–8950. [PubMed: 28756657]

- (28). Mosely JA; Smith MJ; Prakash AS; Sims M; Bristow AW Electron-induced dissociation of singly charged organic cations as a tool for structural characterization of pharmaceutical type molecules *Anal. Chem.* 2011, 83, 4068–4075. [PubMed: 21473579]
- (29). Lemmnitzer K; Riemer T; Groessl M; Su R; Knochenmuss R; Schiller J Comparison of ion mobility-mass spectrometry and pulsed-field gradient nuclear magnetic resonance spectroscopy for the differentiation of chondroitin sulfate isomers *Analytical Methods* 2016, 8, 8483–8491.
- (30). Poyer S; Lopin-Bon C; Jacquinet JC; Salpin JY; Daniel R Isomer separation and effect of the degree of polymerization on the gas-phase structure of chondroitin sulfate oligosaccharides analyzed by ion mobility and tandem mass spectrometry *Rapid Commun. Mass Spectrom.* 2017, 31, 2003–2010. [PubMed: 28901031]
- (31). Schenauer MR; Meissen JK; Seo Y; Ames JB; Leary JA Heparan Sulfate Separation, Sequencing, and Isomeric Differentiation: Ion Mobility Spectrometry Reveals Specific Iduronic and Glucuronic Acid-Containing Hexasaccharides *Anal. Chem.* 2009, 81, 10179–10185. [PubMed: 19925012]
- (32). Kailemia MJ; Park M; Kaplan DA; Venot A; Boons G-J; Li L; Linhardt RJ; Amster IJ High-field asymmetric-waveform ion mobility spectrometry and electron detachment dissociation of isobaric mixtures of glycosaminoglycans *J. Am. Soc. Mass. Spectrom.* 2014, 25, 258–268. [PubMed: 24254578]
- (33). Seo Y; Andaya A; Leary JA Preparation, Separation, and Conformational Analysis of Differentially Sulfated Heparin Octasaccharide Isomers Using Ion Mobility Mass Spectrometry *Anal. Chem.* 2012, 84, 2416–2423. [PubMed: 22283665]
- (34). Seo Y; Schenauer MR; Leary JA Biologically relevant metal-cation binding induces conformational changes in heparin oligosaccharides as measured by ion mobility mass spectrometry *Int. J. Mass spectrom.* 2011, 303, 191–198. [PubMed: 21731426]
- (35). Khanal N; Masellis C; Kamrath MZ; Clemmer DE; Rizzo TR Glycosaminoglycan analysis by cryogenic messenger-tagging IR spectroscopy combined with IMS-MS *Anal. Chem.* 2017, 89, 7601–7606. [PubMed: 28636333]
- (36). Agyekum I; Zong C; Boons G-J; Amster IJ Single Stage Tandem Mass Spectrometry Assignment of the C-5 Uronic Acid Stereochemistry in Heparan Sulfate Tetrasaccharides using Electron Detachment Dissociation *J. Am. Soc. Mass. Spectrom.* 2017, 28, 1741–1750. [PubMed: 28389983]
- (37). Wolff JJ; Amster IJ; Chi L; Linhardt RJ Electron Detachment Dissociation of Glycosaminoglycan Tetrasaccharides *J. Am. Soc. Mass. Spectrom.* 2007, 18, 234–244. [PubMed: 17074503]
- (38). Wolff JJ; Chi L; Linhardt RJ; Amster IJ Distinguishing glucuronic from iduronic acid in glycosaminoglycan tetrasaccharides by using electron detachment dissociation *Anal. Chem.* 2007, 79, 2015–2022. [PubMed: 17253657]
- (39). Huang Y; Yu X; Mao Y; Costello CE; Zaia J; Lin C De novo sequencing of heparan sulfate oligosaccharides by electron-activated dissociation *Anal. Chem.* 2013, 85, 11979–11986. [PubMed: 24224699]
- (40). Leach FE; Riley NM; Westphall MS; Coon JJ; Amster IJ Negative Electron Transfer Dissociation Sequencing of Increasingly Sulfated Glycosaminoglycan Oligosaccharides on an Orbitrap Mass Spectrometer *J. Am. Soc. Mass. Spectrom.* 2017, 1–11.
- (41). Wolff JJ; Leach FE; Laremore TN; Kaplan DA; Easterling ML; Linhardt RJ; Amster IJ Negative electron transfer dissociation of glycosaminoglycans *Anal. Chem.* 2010, 82, 3460–3466. [PubMed: 20380445]
- (42). Wu J; Wei J; Hogan JD; Chopra P; Joshi A; Lu W; Klein J; Boons G-J; Lin C; Zaia J Negative Electron Transfer Dissociation Sequencing of 3-O-Sulfation-Containing Heparan Sulfate Oligosaccharides *J. Am. Soc. Mass. Spectrom.* 2018, 1–11.
- (43). Oh HB; Leach FE; Arungundram S; Al-Mafraji K; Venot A; Boons G-J; Amster IJ Multivariate Analysis of Electron Detachment Dissociation and Infrared Multiphoton Dissociation Mass Spectra of Heparan Sulfate Tetrasaccharides Differing Only in Hexuronic acid Stereochemistry *J. Am. Soc. Mass. Spectrom.* 2011, 22, 582–590. [PubMed: 21472576]

- (44). Shvartsburg AA; Smith RD Scaling of the resolving power and sensitivity for planar FAIMS and mobility-based discrimination in flow-and field-driven analyzers *J. Am. Soc. Mass. Spectrom.* 2007, 18, 1672–1681. [PubMed: 17723907]
- (45). Clowers BH; Hill HH Mass analysis of mobility-selected ion populations using dual gate, ion mobility, quadrupole ion trap mass spectrometry *Anal. Chem.* 2005, 77, 5877–5885. [PubMed: 16159117]
- (46). Zucker SM; Lee S; Webber N; Valentine SJ; Reilly JP; Clemmer DE An ion mobility/ion trap/ photodissociation instrument for characterization of ion structure *J. Am. Soc. Mass. Spectrom.* 2011, 22, 1477. [PubMed: 21953250]
- (47). Hernandez DR; DeBord JD; Ridgeway ME; Kaplan DA; Park MA; Fernandez-Lima F Ion dynamics in a trapped ion mobility spectrometer *Analyst* 2014, 139, 1913–1921. [PubMed: 24571000]
- (48). Michelmann K; Silveira JA; Ridgeway ME; Park MA Fundamentals of trapped ion mobility spectrometry *J. Am. Soc. Mass. Spectrom.* 2015, 26, 14–24. [PubMed: 25331153]
- (49). Adams KJ; Montero D; Aga D; Fernandez-Lima F Isomer separation of polybrominated diphenyl ether metabolites using nanoESI-TIMS-MS *International Journal for Ion Mobility Spectrometry* 2016, 19, 69–76. [PubMed: 27642261]
- (50). Benigni P; Thompson CJ; Ridgeway ME; Park MA; Fernandez-Lima F Targeted High-Resolution Ion Mobility Separation Coupled to Ultrahigh-Resolution Mass Spectrometry of Endocrine Disruptors in Complex Mixtures *Anal. Chem.* 2015, 87, 4321–4325. [PubMed: 25818070]
- (51). Schenk ER; Mendez V; Landrum JT; Ridgeway ME; Park MA; Fernandez-Lima F Direct observation of differences of carotenoid polyene chain cis/trans isomers resulting from structural topology *Anal. Chem.* 2014, 86, 2019–2024. [PubMed: 24428664]
- (52). Jeanne Dit Fouque K; Garabedian A; Porter J; Baird M; Pang X; Williams TD; Li L; Shvartsburg A; Fernandez-Lima F Fast and Effective Ion Mobility–Mass Spectrometry Separation of d-Amino-Acid-Containing Peptides *Anal. Chem.* 2017, 89, 11787–11794. [PubMed: 28982001]
- (53). Pu Y; Ridgeway ME; Glaskin RS; Park MA; Costello CE; Lin C Separation and identification of isomeric glycans by selected accumulation-trapped ion mobility spectrometry–electron activated dissociation tandem mass spectrometry *Anal. Chem.* 2016, 88, 3440–3443. [PubMed: 26959868]
- (54). Ridgeway ME; Wolff JJ; Silveira JA; Lin C; Costello CE; Park MA Gated trapped ion mobility spectrometry coupled to fourier transform ion cyclotron resonance mass spectrometry *International Journal for Ion Mobility Spectrometry* 2016, 19, 77–85. [PubMed: 27667964]
- (55). Benigni P; Porter J; Ridgeway ME; Park MA; Fernandez-Lima F Increasing Analytical Separation and Duty Cycle with Nonlinear Analytical Mobility Scan Functions in TIMS-FT-ICR MS *Anal. Chem.* 2018, 90, 2446–2450. [PubMed: 29376337]
- (56). Arungundram S; Al-Mafraji K; Asong J; Leach FE, III; Amster IJ; Venot A; Turnbull JE; Boons G-J Modular synthesis of heparan sulfate oligosaccharides for structure– activity relationship studies *J. Am. Chem. Soc.* 2009, 131, 17394–17405. [PubMed: 19904943]
- (57). Ceroni A; Maass K; Geyer H; Geyer R; Dell A; Haslam SM GlycoWorkbench: A Tool for the Computer-Assisted Annotation of Mass Spectra of Glycans *Journal of Proteome Research* 2008, 7, 1650–1659. [PubMed: 18311910]
- (58). Domon B; Costello CE A systematic nomenclature for carbohydrate fragmentations in FAB-MS/MS spectra of glycoconjugates *Glycoconjugate J.* 1988, 5, 397–409.
- (59). Håkansson K; Axelsson J; Palmblad M; Håkansson P Mechanistic studies of multipole storage assisted dissociation *J. Am. Soc. Mass. Spectrom.* 2000, 11, 210–217. [PubMed: 10697816]
- (60). Sannes-Lowery KA; Hofstadler SA Characterization of multipole storage assisted dissociation: Implications for electrospray ionization mass spectrometry characterization of biomolecules *J. Am. Soc. Mass. Spectrom.* 2000, 11, 1–9. [PubMed: 10631658]
- (61). Sannes-Lowery K; Griffey RH; Kruppa GH; Speir JP; Hofstadler SA Multipole storage assisted dissociation, a novel in–source dissociation technique for electrospray ionization generated ions *Rapid Commun. Mass Spectrom.* 1998, 12, 1957–1961. [PubMed: 9842743]
- (62). Liu FC; Kirk SR; Bleiholder C On the structural denaturation of biological analytes in trapped ion mobility spectrometry–mass spectrometry *Analyst* 2016, 141, 3722–3730. [PubMed: 26998732]

- (63). Zaia J; Li X-Q; Chan S-Y; Costello CE Tandem mass spectrometric strategies for determination of sulfation positions and uronic acid epimerization in chondroitin sulfate oligosaccharides J. Am. Soc. Mass. Spectrom. 2003, 14, 1270–1281. [PubMed: 14597117]
- (64). Hitchcock AM; Costello CE; Zaia J Glycoform Quantification of Chondroitin/Dermatan Sulfate Using a Liquid Chromatography–Tandem Mass Spectrometry Platform Biochemistry 2006, 45, 2350–2361. [PubMed: 16475824]
- (65). Leach FE; Arungundram S; Al-Mafraji K; Venot A; Boons G-J; Amster IJ Electron detachment dissociation of synthetic heparan sulfate glycosaminoglycan tetrasaccharides varying in degree of sulfation and hexuronic acid stereochemistry Int. J. Mass spectrom. 2012, 330–332, 152–159.

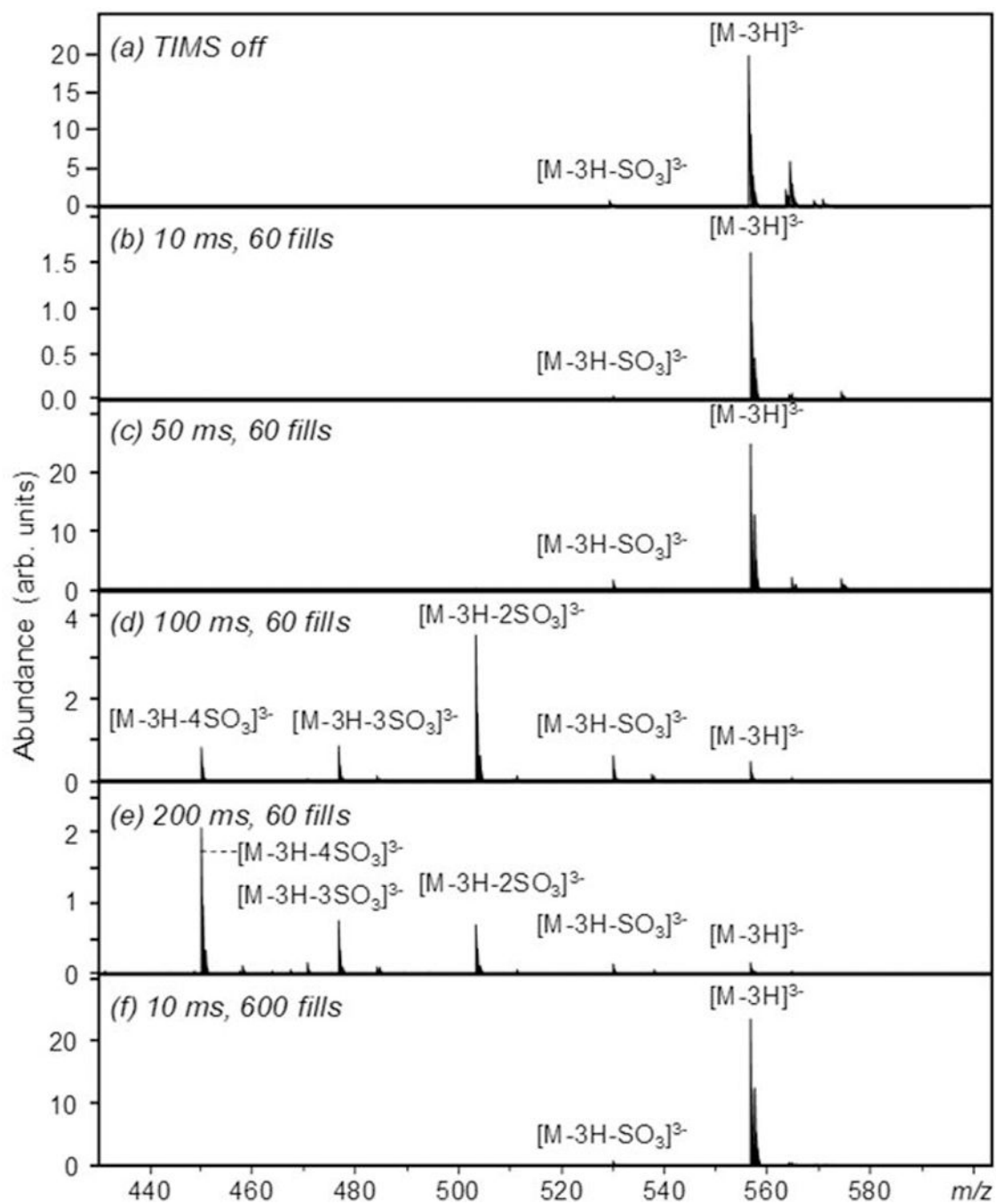


Figure 1.

(a) Mass spectra of Compound 3 acquired in the transmission mode (TIMS off); (b-f) averaged mass spectra of Compound 3 acquired with different TIMS accumulation times and number of collision cell fills.

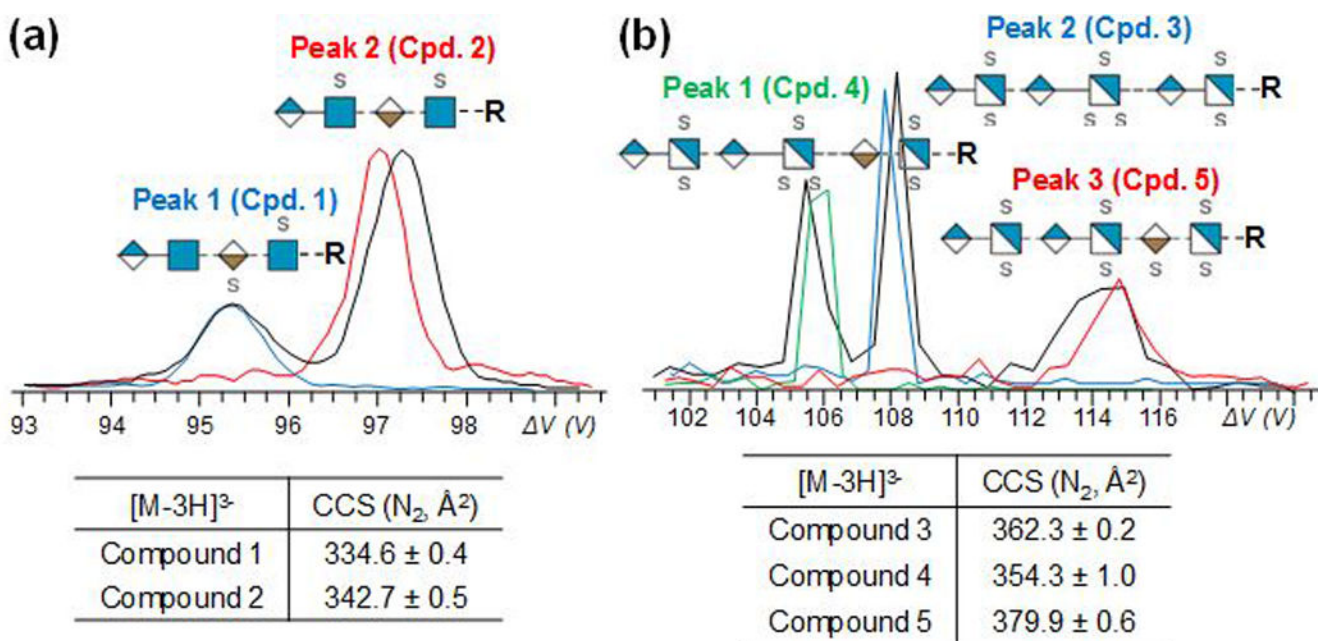


Figure 2. Gated-TIMS separation of two sets of dp4 and dp6 isomers. (a) EIMS ($[M-3H]^{3-}$) of Compound 1 (blue trace), Compound 2 (red trace), and their mixture (black trace); (b) EIMS ($[M-3H]^{3-}$) of Compound 3 (blue trace), Compound 4 (green trace), Compound 5 (red trace), and their mixture (black trace). Averaged CCS values of each compound from three measurements are listed with their standard deviations below the EIMS. R = C₅H₁₀NH₂.

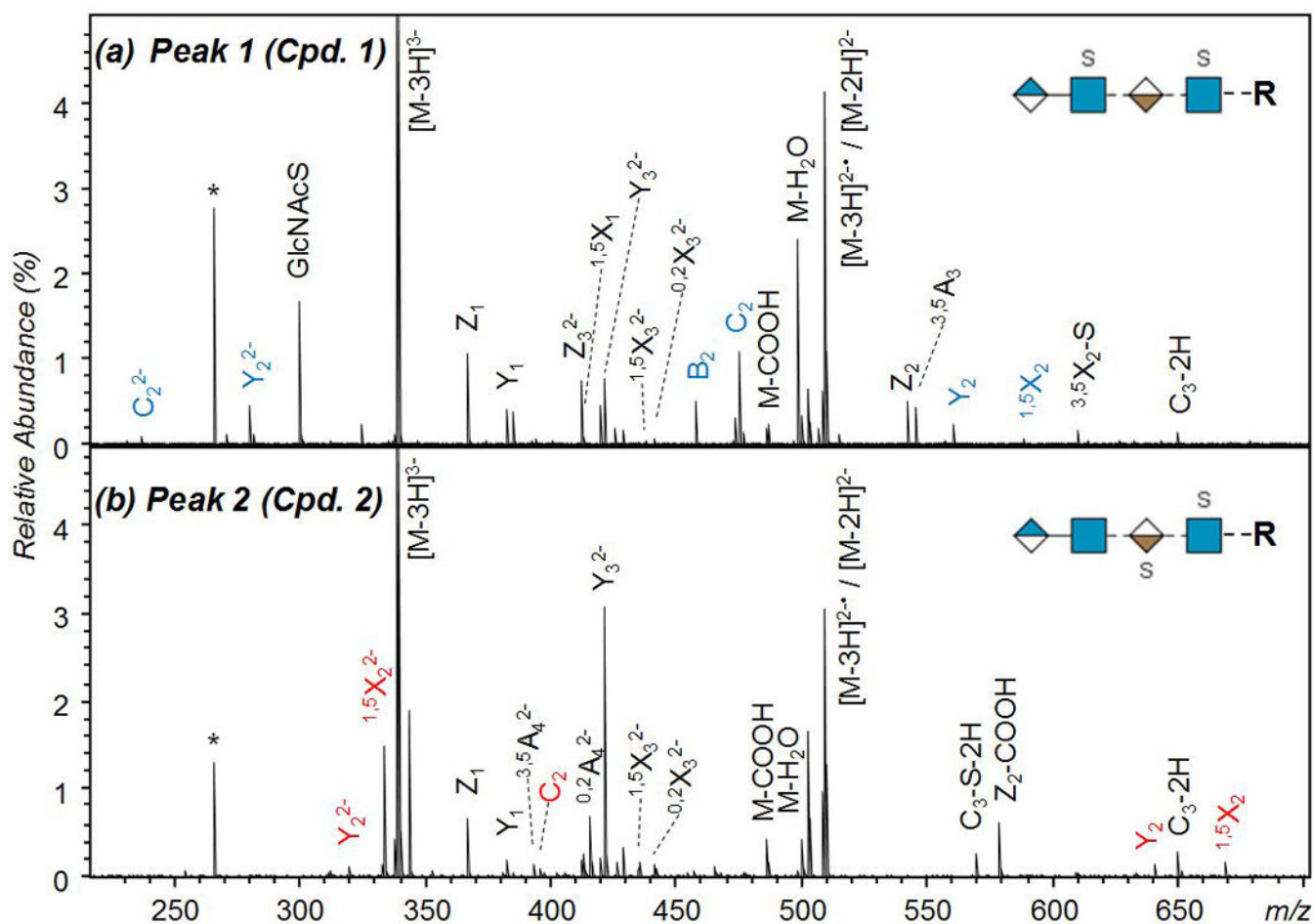


Figure 3.

Gated-TIMS NETD MS/MS analysis of a mixture of Compounds 1 and 2 in the 3- charge state. (a) and (b) are the NETD spectra of peak 1 and peak 2, respectively, in Figure 2a.

Asterisks mark the electronic noise. Measured m/z values for assigned peaks are shown in Supplementary Tables S2 and S3. $R = C_5H_{10}NH_2$.

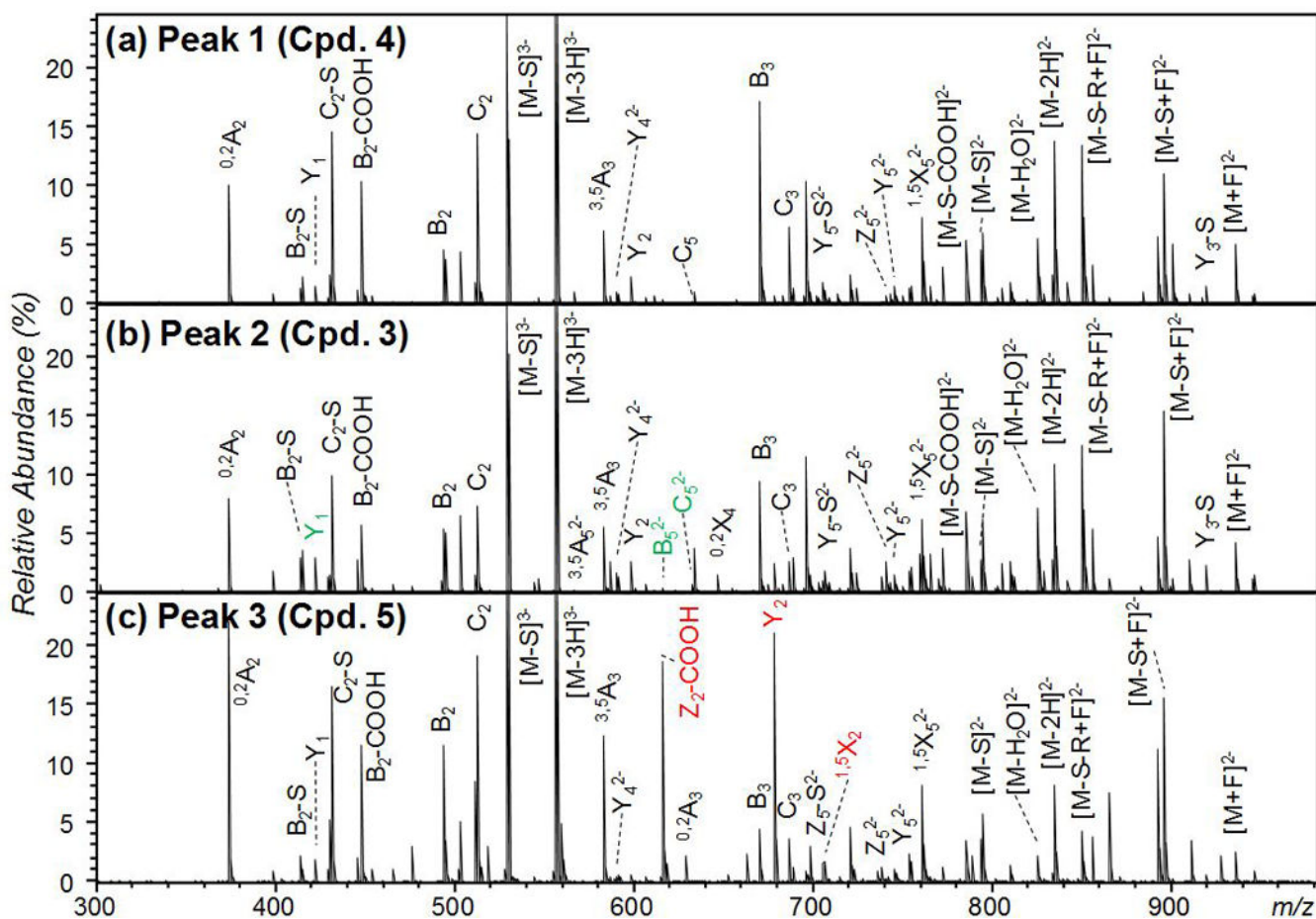


Figure 4. Gated-TIMS NETD MS/MS analysis of a mixture of Compounds 3, 4 and 5 in the 3- charge state. (a-c) NETD spectra of peaks 1, 2, and 3, respectively, in Figure 2b. Sulfo losses are labeled as $-S$, fluoranthene adducts are indicated by $+F$, and the loss of the aminopentyl group is marked by $-R$. Measured m/z values for assigned peaks are shown in Supplementary Tables S4 – S6.

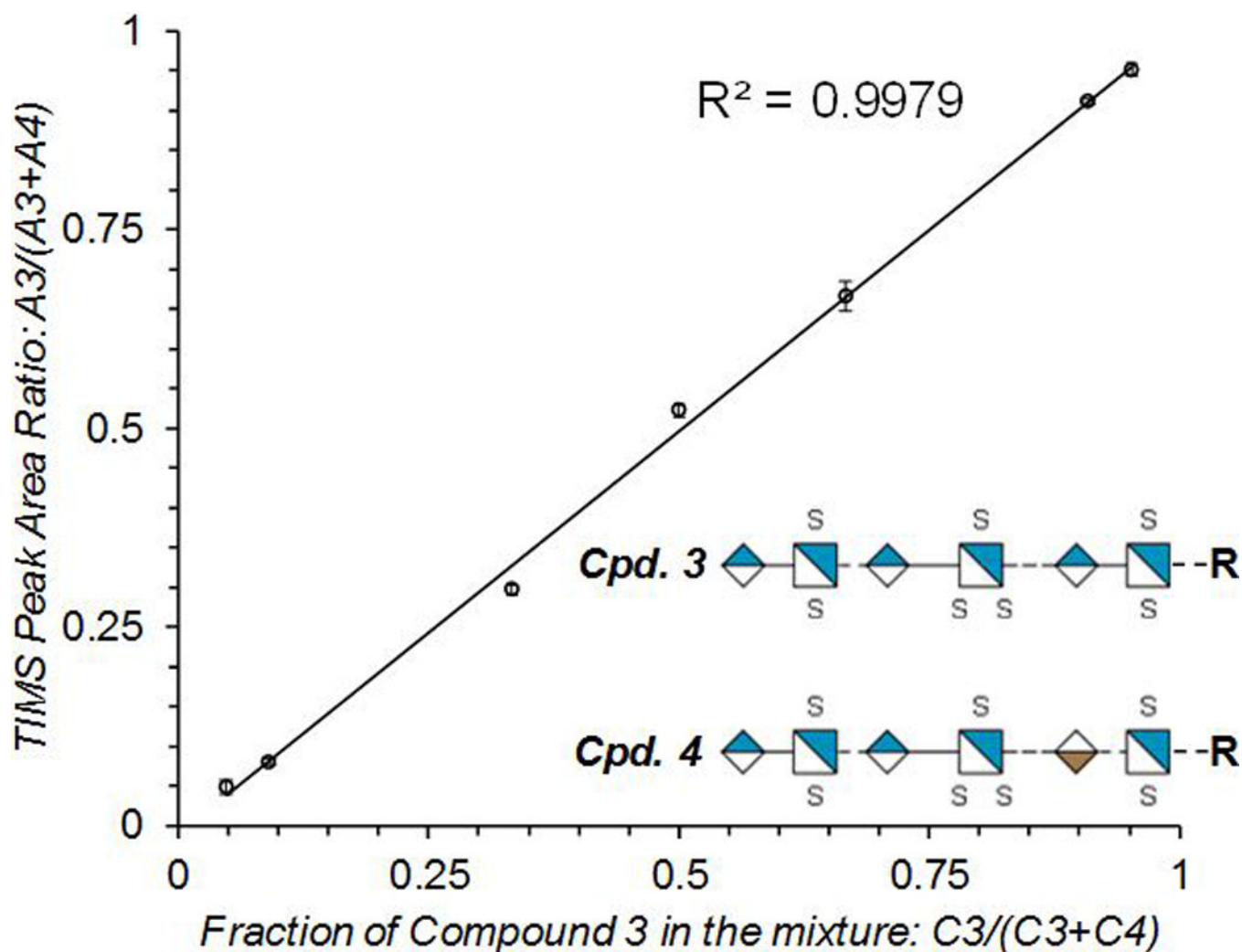


Figure 5.

Relative quantification of two dp6 stereoisomers. The peak area ratio, $A_3/(A_3+A_4)$, was averaged over three technical replicates, and plotted against the ratio of the concentration of Compound 3 over the total concentration, $C_3/(C_3+C_4)$. Error bars show the standard deviations of three measurements (generally less than 2%). Data used to generate this plot can be found in Supplementary Table S7. R = $C_5H_{10}NH_2$.